*ASSOCIAÇÃO BRASILEIRA DE ENERGIA NUCLEAR – ABEN*
*2019 International Nuclear Atlantic Conference - INAC 2019*
*Santos, SP, Brazil, October 21-25, 2019*

Agência Brasileira do ISBN
ISBN 978-85-99141-08-3

# DEVELOPMENT OF NEUTRON SHIELDING FOR AN INERTIAL ELECTROSTATIC CONFINEMENT NUCLEAR FUSION DEVICE

**Seung M. Lee, Helio Yoriyaz and Eduardo L. L. Cabral**

Instituto de Pesquisas Energéticas e Nucleares (IPEN / CNEN - SP)
Av. Professor Lineu Prestes 2242
05508-000 São Paulo, SP, Brazil
smlee@ipen.br; hyoriyaz@ipen.br; elcabral@ipen.br

## ABSTRACT

This work aims to develop a suitable neutron shielding for an Inertial Electrostatic Confinement Nuclear Fusion device (IECF). Neutrons are generated in the IECF device as results of nuclear fusion reactions and their detection is fundamental for the development of the IECF device, because experimental data is needed to perform efficiency analysis and model validation. Nevertheless, it is essential to moderate the neutrons down to the thermal state to make it possible to detect those using conventional detectors. Therefore, to properly measure the fast neutron generation rate by the IECF device it is necessary to previously elaborate a detailed neutron transport model between the IECF device and the radiation shielding, where the neutron detector will be located. In this work, a model is elaborated using the Monte Carlo N-Particle Code and is used to design the required radiation shielding for the device. Later, the same model will be used to determine the proportionality factor between the fast neutron generation in the IECF device and the thermal neutron population in the shielding.

## 1. INTRODUCTION

This work is part of the development of a new type of Inertial Electrostatic Confinement Nuclear Fusion device (IECF) [1-4] and aims to develop a suitable shielding for neutrons generated as result of fusion reactions. This work will also be applied for developing a neutron detection system for the IECF device. Neutron detection is essential for the development of this kind of devices; due to the fact that getting the experimental data of the device in operation is necessary to enable its efficiency analysis and models validation. The main problem is that the neutrons generated by nuclear fusion reactions are fast neutrons so that their detection and counting are difficult using common detectors. Therefore, the first step for detection of those neutrons is to moderate them down to the thermal state and it means that the radiation shielding for the device must have a layer of moderator, thick enough to assure the thermalization of the neutrons. Once done, a population of thermal neutrons is created inside the shielding wall as a result of thermalization and its scale is proportional to the fast neutrons generation rate; however, this proportionality varies with the experimental arrangement. Therefore, it is important to elaborate firstly a detailed neutron transport model between the IECF device and the detector along the shielding. In this context, a transport model is elaborated for the Monte Carlo N-Particle Code (MCNP) [5-7]; this model will enable the determination of the proportionality between the detected thermal neutrons and the fast neutrons which are generated in the device. Furthermore, this model is applied to design the required radiation shield for the safe operation of the device. In this context, this work is carried out in two stages: (1) development of a neutron transport model using the MCNP code to simulate the interaction of the neutrons generated inside the IECF device with the surrounding materials; and (2) determination of suitable dimensions and

materials of the radiation shielding for the device. The results of this work will enable in the future defining the main parameters of the neutron detection system for the IECF device.

## 2. METHODOLOGY

A preliminary scheme of the experimental arrangement of the area where the IECF device will be installed is presented in Figure 1, which shows also various auxiliary systems of the device and the radiation shielding.

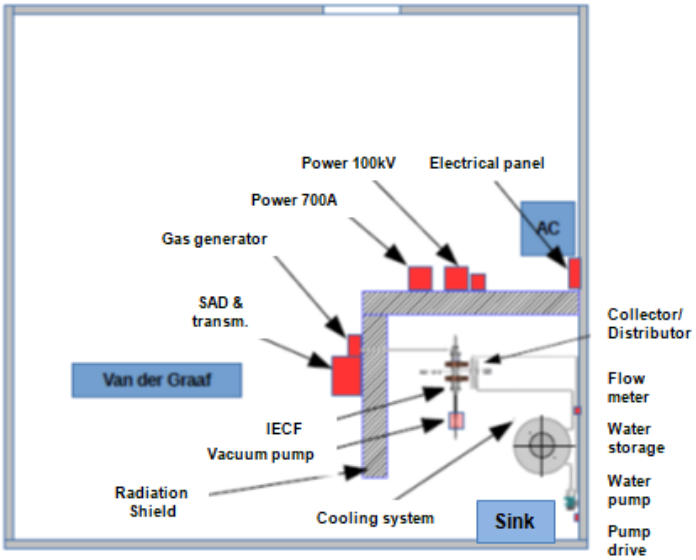


**Figure 1: Illustration of the laboratory of the IECF device.**

The problem was modeled in 12 cells of simple geometries delimited by 11 surfaces, and with 7 materials. Figure 2 shows the layout of the experiment room as it was modeled in *Inp File*. In this figure, the IECF device is represented by a cylinder surrounded by a cubic shielding, both of which are virtually fixed in the air.

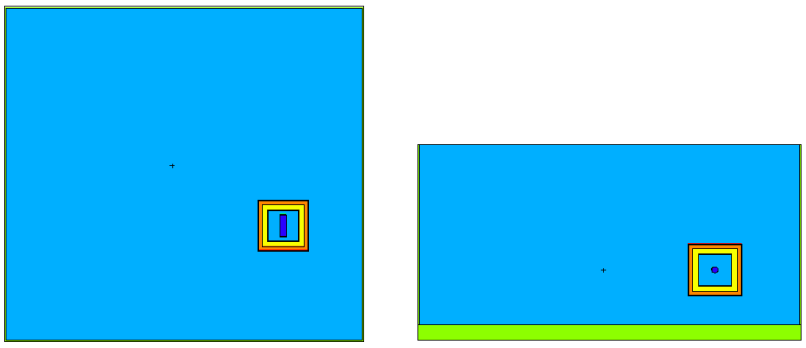

**(a) Top view (XY-plane)** **(a) Side view (XZ-plane)**

**Figure 2: Simplified modelling of the laboratory for MCNP simulation.**

The IECF device was modeled as a cylindrical stainless steel shell containing deuterium ($D_2$) at low pressure as shown in Figure 3. The green region stands for the internal space of the device filled with deuterium, where the nuclear fusion reactions take place; while the gray region represents the stainless steel shell. This is a quite simplified model so that even the cylindrical cathode grid, present at the center of the real device, is omitted.

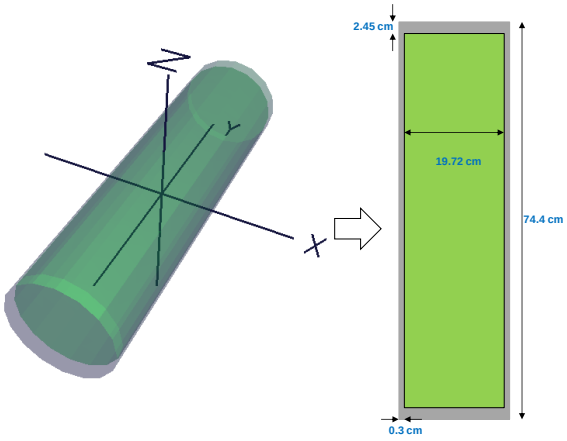


**Figure 3: Simplified model of IECF for MCNP simulation.**

The IECF device is surrounded by a multi-layered cubic shield consisting of three types of materials: 1) fast neutron moderator; 2) thermal neutron absorber; and 3) structural materials. As neutrons moderator, paraffin $C_{31}H_{64}$ ($\rho$=0,9g/cm$^3$) is chosen; and as thermal neutron absorber, boric acid, $H_3BO_3$ ($\rho$=1,435g/cm$^3$). The densities of the structural materials, i.e., stainless steel and wood, are assumed to be 7,86g/cm$^3$ [7] and 0,7g/cm$^3$ [8], respectively. The arrangement of shielding of one of the simulated cases is shown in Figure 4. Simulations were carried out varying the thickness of the layers of paraffin and boric acid, while the distance between the IECF and the inner surface of the shield was fixed at 50cm in all cases.

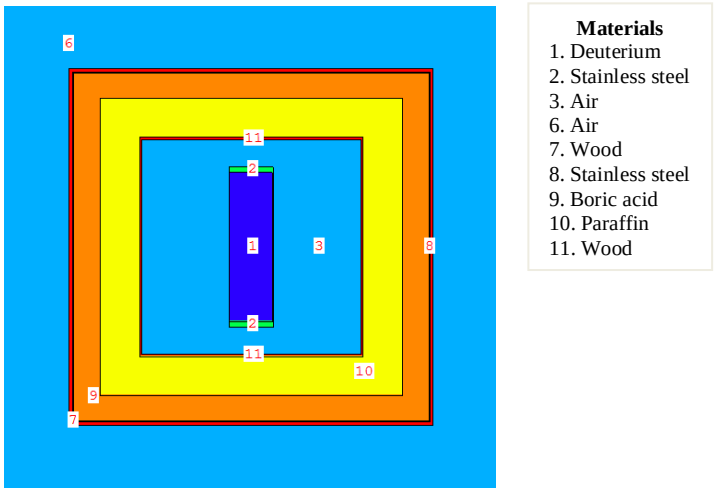


**Figure 4: The IECF shield scheme (XY-plane)**

The wall, ceiling and floor of the laboratory are assumed to be of the same material, typical concrete [7] ($\rho$=2.3g/cm$^3$). The list of materials used in the simulations is presented below in Table 1.

**Table 1: List of materials implemented in the simulation.**

| Material | Composition (weight fraction) | | Density (g/cm$^3$) | Chemical formula | Application |
|---|---|---|---|---|---|
| Deuterium | D | 1.0 | 1.0E-5 | $D_2$ | IECF |
| Air | N | 0.755 | 0.001 | - | Interior (Lab. and shielding) |
| | O | 0.231 | | | |
| | Ar | 0.014 | | | |
| Stainless Steel. | C | 0.00075 | 7.86 | - | IECF, Shielding (structural) |
| | N | 0.00125 | | | |
| | Si | 0.00500 | | | |
| | P | 0.00030 | | | |
| | S | 0.00015 | | | |
| | Cr | 0.18000 | | | |
| | Mn | 0.08750 | | | |
| | Fe | 0.67505 | | | |
| | Ni | 0.05000 | | | |
| Concrete | H | 0.00600 | 2.35 | - | wall, ceiling, floor |
| | O | 0.50000 | | | |
| | Na | 0.01700 | | | |
| | Al | 0.04800 | | | |
| | $^{28}$Si | 0.28940 | | | |
| | $^{29}$Si | 0.01518 | | | |
| | $^{30}$Si | 0.01042 | | | |
| | K | 0.01900 | | | |
| | Ca | 0.08300 | | | |
| | $^{54}$Fe | 0.00068 | | | |
| | $^{56}$Fe | 0.01106 | | | |
| | $^{57}$Fe | 0.00026 | | | |
| Paraffin | H | 0.85817 | 0.9 | $C_{31}H_{64}$ | Shielding (Moderator) |
| | C | 0.14183 | | | |
| Boric acid | H | 0.04891 | 1.435 | $H_3BO_3$ | Shielding (Absorber) |
| | B | 0.17483 | | | |
| | O | 0.77626 | | | |
| Wood (cellulose [a]) | H | 0.06217 | 0.7 | $C_6H_{10}O_5$ | Shielding (structural) |
| | C | 0.44446 | | | |
| | O | 0.49337 | | | |

[a] The density of cellulose was reduced from 1,5g/cm$^3$ to 0,7g/cm$^3$.

Inside the IECF device in operation fast neutrons are generated as result of nuclear fusions, so that its interior can be considered as a source of those neutrons, whose intensity is proportional to the number of fusion reactions. Since the model of the IECF dealt with here is a simple cylindrical shell containing deuterium at low pressure, without a cathode inside, it is assumed to be a homogeneous and isotopic source of fast neutrons, whose intensity can be chosen by user. In the present work, the intensity of the source is assumed to be $10^{12}$ neutrons/s.

In order to calculate the radiation doses caused by neutrons outside the shield, three imaginary ring type detectors were implemented as illustrated in Figure 5. These rings have radius of 150cm and are aligned with the Y-axis as well as the IECF device itself. The

coordinates of the centers of these detectors, $D_0$, $D_{20}$, $D_{40}$, are respectively, (0, 0, 0), (0, 20, 0) and (0, 40, 0), given in centimeter.

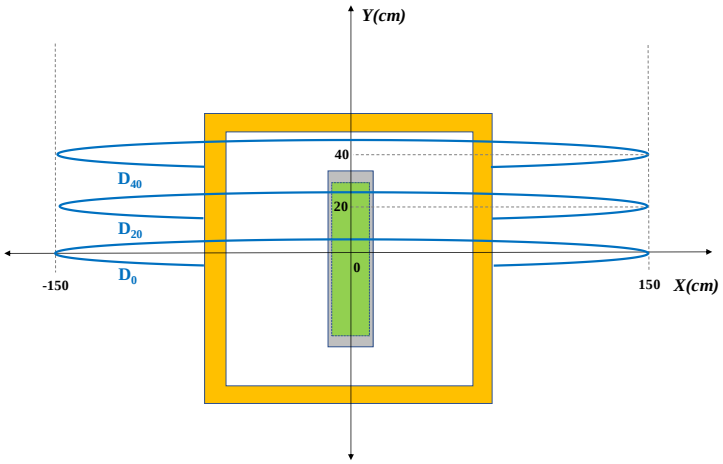


**Figure 5: Disposition of the ring type detectors: $D_0$, $D_{20}$ and $D_{40}$.**

The radiation doses were calculated varying the thickness of both the paraffin and boric acid layers. Figure 6 illustrates a cross-sectional view of the shielding, where $\alpha$ and $\beta$ stand for the paraffin and boric acid thickness, respectively. Obviously, the total thickness of the shielding varies with $\alpha$ and $\beta$, but the distance between the center of the device and the inner surface of the shield remains constant.

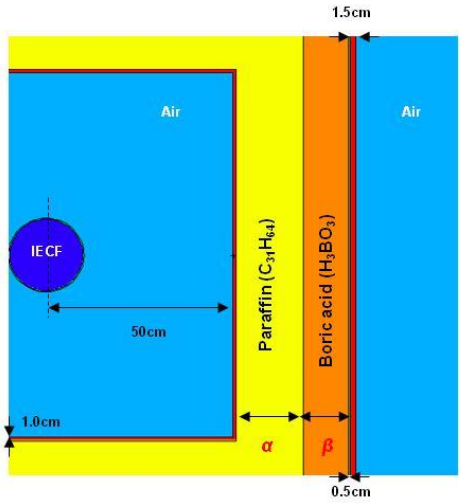


**Figure 6: The cross-sectional view of the shield, where $\alpha$ and $\beta$ are variables.**

The values for $\alpha$ and $\beta$ were chosen so that the number of atoms of boron is approximately 5% along the two main layers of the shield. Table 2 lists the dimension of all the layers of the shielding, with which the simulations were carried out.

**Table 2: Dimensions of the radiation shield**

| Total thickness (cm) | Paraffin, $\alpha$ (cm) | Boric acid $\beta$ (cm) | B atoms (%) | Inner wood (cm) | Outer wood (cm) | Stainless steel (cm) |
|---|---|---|---|---|---|---|
| **30,5** | 16,5 | 11 | 5,09 | 1,0 | 1,5 | 0,5 |
| **33,0** | 18,0 | 12 | | | | |
| **35,5** | 19,5 | 13 | | | | |
| **38,0** | 21,0 | 14 | | | | |
| **40,5** | 22,5 | 15 | | | | |
| **43,0** | 24,0 | 16 | | | | |
| **45,5** | 25,5 | 17 | | | | |
| **48,0** | 27,0 | 18 | | | | |
| **50,5** | 28,5 | 19 | | | | |
| **53,0** | 30,0 | 20 | | | | |
| **55,5** | 31,5 | 21 | | | | |
| **58,0** | 33,0 | 22 | | | | |
| **60,5** | 34,5 | 23 | | | | |
| **63,0** | 36,0 | 24 | | | | |

The input files for these simulations are set in order that the radiation dose are calculated in biological dose equivalent rate, i.e., in [rem/h]. For these calculations, it was used the set of neutron flux-to-dose rate conversion factors and quality factors of the National Council on Radiation Protection and Measurements [7], NCRP-38. These conversion factors as well as the quality factors are listed in Table 3. Furthermore, for convenience, the initial energy of all the fast neutrons was assumed to be 2,5MeV.

**Table 3: Neutron Flux-to-Dose Rate Conversion Factors and Quality Factors [7].**

| **Energy of neutrons** (MeV) | **Flux-to-dose conversion factors** (rem/h)/(n/cm$^2$·s) | **Quality factors** |
|---|---|---|
| **2.5E-8** | 3.67E-6 | 2,0 |
| **1.0E-7** | 3.67E-6 | 2,0 |
| **1.0E-6** | 4.46E-6 | 2,0 |
| **1.0E-5** | 4.54E-6 | 2,0 |
| **1.0E-4** | 4.18E-6 | 2,0 |
| **1.0E-3** | 3.72E-6 | 2,0 |
| **1.0E-2** | 3.56E-6 | 2,0 |
| **1.0E-1** | 2.17E-5 | 7,5 |
| **5.0E-1** | 9.26E-5 | 11,0 |
| **1.0** | 1.32E-4 | 11,0 |
| **2.5** | 1.25E-4 | 9,0 |

Source: American National Standard ANSI/ANS-6.1.1-1977.

## 3. RESULTS

The equivalent dose rates thus calculated and their uncertainties for all detectors are listed in Table 4, which are the results of the averages of the $10^7$ particle stories, or number of particle stories, *nps*. As expected, the highest radiation dose rates is recorded in detector $D_0$ positioned near the center of the device, while the lowest is recorded in detector $D_{40}$, the farthest from the center.

**Table 4: Calculated Doses Equivalent Rates**.

| Total thickness (cm) | $D_0$ (rem/h) | $\sigma_0$ | $D_{20}$ (rem/h) | $\sigma_{20}$ | $D_{40}$ (rem/h) | $\sigma_{40}$ |
|---|---|---|---|---|---|---|
| **30,5** | 3.13E+00 | 0.0055 | 2.96E+00 | 0.0057 | 2.52E+00 | 0.0060 |
| **33,0** | 1.83E+00 | 0.0072 | 1.72E+00 | 0.0073 | 1.47E+00 | 0.0079 |
| **35,5** | 1.07E+00 | 0.0096 | 1.01E+00 | 0.0098 | 8.42E-01 | 0.0105 |
| **38,0** | 6.31E-01 | 0.0126 | 5.90E-01 | 0.0128 | 4.93E-01 | 0.0142 |
| **40,5** | 3.77E-01 | 0.0168 | 3.63E-01 | 0.0176 | 2.92E-01 | 0.0183 |
| **43,0** | 2.21E-01 | 0.0271 | 2.04E-01 | 0.0267 | 1.67E-01 | 0.0295 |
| **45,5** | 1.30E-01 | 0.0303 | 1.18E-01 | 0.0308 | 9.95E-02 | 0.0330 |
| **48,0** | 7.90E-02 | 0.0389 | 7.27E-02 | 0.0406 | 6.10E-02 | 0.0467 |
| **50,5** | 4.58E-02 | 0.0569 | 4.50E-02 | 0.0591 | 3.37E-02 | 0.0631 |
| **53,0** | 2.45E-02 | 0.0662 | 2.04E-02 | 0.0643 | 1.91E-02 | 0.0810 |
| **55,5** | 1.73E-02 | 0.0870 | 1.69E-02 | 0.1015 | 1.24E-02 | 0.1119 |
| **58,0** | 1.01E-02 | 0.1327 | 9.66E-03 | 0.1438 | 7.77E-03 | 0.1332 |
| **60,5** | 6.04E-03 | 0.1509 | 4.96E-03 | 0.1702 | 3.41E-03 | 0.1533 |
| **63,0** | 2.20E-03 | 0.2454 | 4.54E-03 | 0.5714 | 2.28E-03 | 0.2981 |

The dose rates as function of shield thickness are shown in Figure 7, where it can be observed that the increase of shielding thickness does not bring a corresponding gain in neutron shield from a point. Thus, the cost-benefit ratio seems to be acceptable up to 53cm.

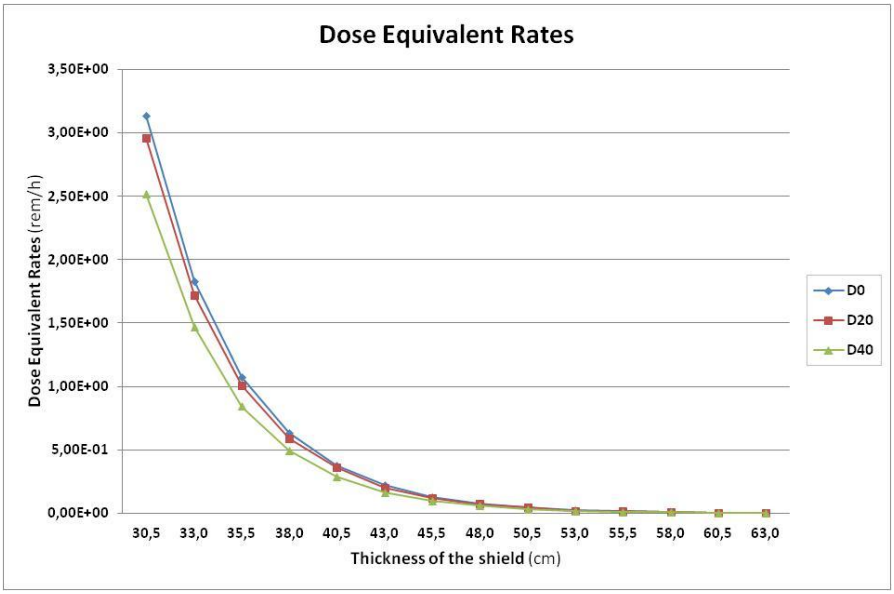


**Figure 7: Doses equivalent rates calculated from the neutron fluxes.**

Furthermore, according to the norm of *Comissão Nacional de Energia Nuclear* (CNEN), the limit of the radiation dose for an individual working in environment with risk of ionizing radiation is 2rems per year, considering that an operator works 2000 hours during this period. Thus, assuming that the IECF device is operated for 5 minutes a day, 5 times a week, for 48 weeks; then, the dose rate limit would be 0.1rem/h according to the norm of CNEN. Therefore, it can be concluded that, based on the operating conditions assumed above for the IECF, a shielding of 48cm, composed of 27cm of layer of paraffin and 18cm of boric acid, would be sufficient to meet the requirement of CNEN.

## 4. CONCLUSIONS

The elaborated input files for the MCNP6 code yielded consistent results for the experimental arrangement used for these initial analyses. The model of both the IECF device and its shielding can be enhanced by including more details of the physical arrangement in order to make the neutron transport calculation more realistic. On the other hand, improvements in the IECF and shielding model would not bring about significant changes in resultant dose rates, as long as neutron emission is assumed to be isotropic. The most important factors in determining radiation shield seem to be the source intensity and the energy of the neutrons emitted from fusion reactions. Therefore, regarding the radiation shielding, the result obtained in this work can be used as a good reference for the future improvements. Finally, it can be purposed as next steps definition of the main parameters of the neutron detection system, as well as calibration of the detectors.

## ACKNOWLEDGMENTS

To *Fundação de Amparos à Pesquisa do Estado de São Paulo* (FAPESP) for financial support.

## REFERENCES

1. R. W. Brussard, "Some Physics considerations of magnetic inertial electrostatic confinement: a new concept for spherical converging-flow fusion," *Fusion Technology*, **Vol. 19**, No. 273.
2. W. M. Nevis, "Can inertial electrostatic confinement work beyond the ion-ion collisional time scale?", *Physics of Plasma*, **Vol. 2**, pp. 1853.
3. T. H. Rider, "A general critique of inertial confinement fusion systems," *Physics of Plasmas*, **Vol.2** (6).
4. M. Rosenberg and N. A. Krall, "The effect of collisions in maintaining a non-Maxwellian plasma distribution in a spherically convergent ion focuses" *Physics of Fluids B*, **Vol. 4** (7).
5. C.J. Werner, et al., *MCNP6.2 Release Notes*, Los Alamos National Laboratory, report LA-UR-18-20808 (2018).
6. C.J. Werner, *MCNP User's Manual - Code Version 6.2*, Los Alamos National Laboratory, report LA-UR-17-29981 (2017).
7. Pelowitzh, Denise B., et al., *MCNP6$^{TM}$ User's Manual. Version 1.0*, Los Alamos National Security, LLC. 2013.
8. Pettersen, Roger C, "The chemical composition of wood". *Advances in Chemistry*, Series 207. Washington, DC. American Chemical Society. Chapter 2. 1984.